Editors' Suggestion

# Composition Dependent Instabilities in Mixtures with Many Components

Filipe C. Thewes,[1,*] Matthias Krüger,[1] and Peter Sollich[1,2]
[1]Institut für Theoretische Physik, Georg-August-Universität Göttingen, 37077 Göttingen, Germany
[2]King's College London, Department of Mathematics, Strand, London WC2R 2LS, United Kingdom

(Received 29 November 2022; revised 28 March 2023; accepted 27 June 2023; published 3 August 2023)

Understanding the phase behavior of mixtures with many components is important in many contexts, including as a key step toward a physics-based description of intracellular compartmentalization. Here, we study phase ordering instabilities in a paradigmatic model that represents the complexity of—e.g., biological—mixtures via random second virial coefficients. Using tools from free probability theory we obtain the exact spinodal curve and the nature of instabilities for a mixture with an arbitrary composition, thus lifting an important restriction in previous work. We show that, by controlling the concentration of only a few components, one can systematically change the nature of the spinodal instability and achieve demixing for realistic scenarios by a strong *composition imbalance amplification*. This results from a nontrivial interplay of interaction complexity and entropic effects due to the nonuniform composition. Our approach can be extended to include additional systematic interactions, leading to a competition between different forms of demixing as density is varied.

DOI: 10.1103/PhysRevLett.131.058401

Phase separation is an important phenomenon and especially rich in mixtures with many components. For example, biological mixtures such as the cytoplasm show complex phase behavior believed to be a key driver in the formation of nucleoli and other intracellular structures [1–5]. Typically, these systems demix into liquid droplets with different compositions, where each phase is enriched in selected components and depleted in others [4,6].

Recent studies [7–11] have explored the behavior of complex mixtures based on the model introduced by Sear and Cuesta [12] where the interactions between components are taken as random. The model captures *typical* effects of complex mixture interactions. It provides a generic maximum entropy description of the distribution of the large number of second virial coefficients in a multicomponent mixture when the mean and variance are known, analogously to the standard, and successful use of random matrices in nuclear physics [13]. Recently, an extended version of the model including systematic interactions has also been used to qualitatively describe experimental results on phase separation triggered by a change in pH in the cytoplasm of eukaryotic cells [14]. Although these studies have been able to illuminate some of the resulting physics, a key restrictive assumption common to all of them is uniform composition, meaning all species are taken to be present in equal amounts. However, biological mixtures rarely satisfy this condition [15–17], and the size of intracellular structures is in fact heavily dependent on the composition of the cytoplasmic pool [18,19].

With this in mind, our aim in this Letter is to open the door to exploring the full composition-dependent physics of complex multicomponent mixtures, within the Sear and Cuesta model [12]. We lift the drastic simplification of uniform composition, significantly broadening the applicability of the approach and pointing towards new experimental protocols. These could exploit our key insight: systematically changing the concentration of only a few components enables one to control the nature of phase ordering instabilities and, as a consequence, the phases that can be formed. Recent experiments already point in this direction [16,20–22], but a theoretical description of the observations, including the strong dependence of the phases formed on a dominant component [20], has been lacking. Our work also makes composition-dependent effects accessible for complex mixtures including polymers or colloids that have (additional) systematic interactions. More generally, while we focus on mixtures here, instabilities in many complex systems can be approached within an analogous random matrix framework. Our approach can accordingly be translated to similar problems in areas as diverse as glass physics, socioeconomics, ecology, and optimization problems [23–28].

*Model and general results.*—We study a homogeneous mixture of $M$ different components, labeled by Greek letters, with interactions described by the second virial coefficients $\epsilon_{\alpha\gamma}$. The mean-field bulk free energy density $f$ is given by [29]

$$f = \frac{1}{2}\sum_{\alpha,\gamma=1}^{M} \rho_\alpha \epsilon_{\alpha\gamma} \rho_\gamma + T\sum_{\alpha=1}^{M} \rho_\alpha \ln \rho_\alpha + T\rho_0 \ln \rho_0, \quad (1)$$

where $\rho_\alpha = N_\alpha/V$ is the number density of species $\alpha$, $T$ is temperature, and we use $k_B = 1$. The last term in (1) is the

 

entropic contribution of an implicit solvent, interacting only via volume exclusion. We define the total density as $\rho = \sum_\alpha \rho_\alpha$, the average density per component as $\bar{\rho} = \rho/M$, and we work with units such that $\rho_0 = 1 - \rho$.

From (1) we obtain the $M \times M$ Hessian matrix $\boldsymbol{H}$ with entries $H_{\alpha\gamma} = \partial^2 f/(\partial\rho_\alpha \partial\rho_\gamma)$. Thermodynamic stability requires all eigenvalues of $\boldsymbol{H}$ to be non-negative. Otherwise, i.e., if the lowest eigenvalue $\lambda_{\min}$ is negative, the system is unstable to phase separation by spinodal decomposition. The corresponding eigenvector $\boldsymbol{v}$ determines the nature of the spinodal instability, with local density fluctuations of the different mixture components $\alpha$ growing proportionally to $\boldsymbol{v}$, $\delta\rho_\alpha \sim v_\alpha$.

The phase diagram in the $(\rho, T)$ plane for a fixed set of *relative densities* $\{y_\alpha = \rho_\alpha/\bar{\rho}\}$ splits into stable and unstable regions, separated by a spinodal line determined by the condition $\lambda_{\min} = 0$ [30]. Close to this line, $\boldsymbol{v}$ is governed only by the bulk free energy and additional interfacial contributions not written in (1) can be neglected. We will be interested in instabilities of *condensation* type ($\boldsymbol{v} \sim \boldsymbol{u}$), with $\boldsymbol{u} = (1, 1\ldots, 1)^\mathsf{T}$, where the densities of all species change by similar amounts, and of *demixing* type ($\boldsymbol{v}^\mathsf{T}\boldsymbol{u} \approx 0$), where some species are enhanced while others are depleted. We will show that the demixing case can be further split into delocalized or *random*, where all components of $\boldsymbol{v}$ are of similar order, and *localized* where a few species have much larger entries in $\boldsymbol{v}$ and thus dominate the demixing.

Following Ref. [12], we model the second virial coefficients $\epsilon_{\alpha\gamma}$ as Gaussian random variables of mean $-b$ and variance $s^2$, drawn independently except for the symmetry constraint $\epsilon_{\alpha\gamma} = \epsilon_{\gamma\alpha}$. With this choice the Hessian matrix reads

$$\boldsymbol{H} = \boldsymbol{R}_1 + \boldsymbol{D} + s\boldsymbol{\eta} \quad \text{with}$$
$$\boldsymbol{R}_1 = \left(-b + \frac{T}{\rho_0}\right)\boldsymbol{u}\boldsymbol{u}^\mathsf{T}, \qquad \boldsymbol{D} = \frac{T}{\bar{\rho}}\,\mathrm{diag}\left(\frac{1}{y_\alpha}\right) \tag{2}$$

and $\boldsymbol{\eta}$ a Wigner matrix with entries of zero mean and unit variance [31], while $\mathrm{diag}(1/y_\alpha)$ is a diagonal matrix with the $1/y_\alpha$ as entries. Understanding phase ordering instabilities then requires us to obtain the eigenvalue distribution or *spectrum* of $\boldsymbol{H}$, and specifically its lower edge $\lambda_{\min}$. We focus throughout on the interesting multicomponent limit $M \gg 1$, where the following analysis in fact applies for generic, non-Gaussian distributions of the $\epsilon_{\alpha\gamma}$ (with the same first four moments [32]).

The $s\boldsymbol{\eta}$ term in $\boldsymbol{H}$ produces a continuous spectrum of eigenvalues, and this extends to $\boldsymbol{D} + s\boldsymbol{\eta}$ [33]. The term $\boldsymbol{R}_1$ is a rank one perturbation to this; due to the interlacing property of eigenvalues [34], the spectrum of $\boldsymbol{H}$ for large $M$ is then either the same as the spectrum of $\boldsymbol{D} + s\boldsymbol{\eta}$, or $\boldsymbol{R}_1$ may give rise to a single outlier [35] separated from the continuous bulk spectrum of eigenvalues. We therefore have two regimes: if an outlier exists to the left of the bulk, then it is the lowest eigenvalue $\lambda_{\min}$. Otherwise the lowest eigenvalue is given by the lower edge of the bulk itself.

Free probability [31,36] is a powerful tool to obtain the statistics of eigenvalues and eigenvectors of large random matrices, provided they obey the so-called freeness criteria. A key insight is that freeness generically holds between $\boldsymbol{D}$, $s\boldsymbol{\eta}$, and $\boldsymbol{R}_1$ [37]. We can thus use free probability to analyze the spectrum of the scaled Hessian $\boldsymbol{H}/M$; adopting also the scaling $s = M^{1/2}\tilde{s}$ [12] ensures all matrices involved have eigenvalues of $O(1)$. We find [37] for the spinodal equation, which determines where $\lambda_{\min} = 0$,

$$\langle (1/y_\alpha - \xi z)^{-1} \rangle = Tz/\rho. \tag{3}$$

The angular brackets denote an average over the distribution $p(y_\alpha)$ of the $y_\alpha$, which specifies the mixture composition, and we have defined $\xi = \rho\tilde{s}^2/T$. Equation (3) is to be solved for $T$ as a function of total density $\rho$. The difference between the outlier and bulk regimes lies in the way $z = z(\rho, T)$ is determined, as we explain next.

First, in the outlier regime one has $z = \theta^{-1}$, where $-\theta = T/\rho_0 - b$ is the nonzero eigenvalue of $\boldsymbol{R}_1/M$; this has to be negative to give rise to an outlier to the left of the bulk, hence the definition as $-\theta$. We can also determine the overlap between the (normalized) instability vector $\boldsymbol{v}$ and the normalized uniform vector $\hat{\boldsymbol{u}} = \boldsymbol{u}/\sqrt{M}$ as

$$|\boldsymbol{v}^\mathsf{T}\hat{\boldsymbol{u}}|^2 = \max\left\{\frac{\langle (1/y_\alpha - \xi\theta^{-1})^{-1}\rangle^2}{\langle (1/y_\alpha - \xi\theta^{-1})^{-2}\rangle} - \frac{\tilde{s}^2}{\theta^2}, 0\right\}. \tag{4}$$

We refer to instabilities with nonvanishing overlap between $\boldsymbol{v}$ and $\hat{\boldsymbol{u}}$ as condensation (C), and as demixing otherwise. Equation (4) thus provides information on the nature of the instability and is one of our key results. The first term inside the max, which is a squared mean over a second moment, is unity for uniform compositions but lower for nonuniform ones. This already suggests that nonuniformity will favor demixing, which we will see confirmed below.

Turning next to the bulk regime, we find that the first argument of the max in (4) is then negative and we have demixing behavior, with the lowest eigenvalue of the bulk $\boldsymbol{D} + s\boldsymbol{\eta}$ governing thermodynamic stability. For the restricted case of uniform composition, $\boldsymbol{D} = (T/\bar{\rho})\boldsymbol{I}$ just shifts the spectrum of $s\boldsymbol{\eta}$ by $T/\bar{\rho}$; the entire demixing regime is then described by a linear spinodal line $T \propto \bar{\rho}$ [12]. For nonuniform composition, on the other hand, the spread of eigenvalues in $\boldsymbol{D}$ can dominate at high enough $T$ [24] as illustrated in Fig. 1. The edge of the bulk of the spectrum is then determined by $\boldsymbol{D}$ and in the spinodal condition (3) one has [37] $z\xi = 1/y_{\max}$, where $y_{\max} = \max_\alpha y_\alpha$. The corresponding eigenvector of $\boldsymbol{D}$ only has a single nonzero entry, and we find as a result that the instability direction $\boldsymbol{v}$ becomes concentrated on a few species. For low enough $T$, on the other hand, the $s\boldsymbol{\eta}$ term dominates in $\boldsymbol{D} + s\boldsymbol{\eta}$ and $z$ has a larger value maximizing a

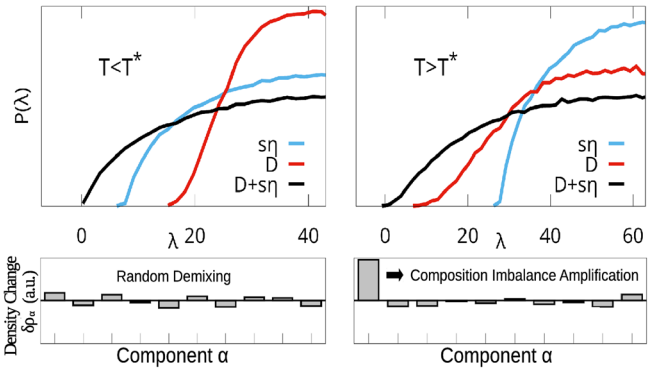


FIG. 1. Top: Example realization of eigenvalue distributions of $\boldsymbol{D}$ and $s\boldsymbol{\eta}$. The lower edge of the spectrum of the sum $\boldsymbol{D}+s\boldsymbol{\eta}$ decays with the same power law as the spectrum of $s\boldsymbol{\eta}$ for $T<T^*$, and of $\boldsymbol{D}$ for $T>T^*$; for ease of visualization the spectra have been shifted to have matching means. Bottom: sketch of density changes $\delta\rho_\alpha$, which are proportional to the eigenvector entries $v_\alpha$, illustrating the localization of the instability on a single component for $T>T^*$.

known function depending only on $\tilde{s}$ and the composition $p(y_\alpha)$ [37]. The threshold temperature $T^*$ separating these two cases (see Fig. 1) is given explicitly by

$$T^* = \tilde{s}\rho y_{\max}\sqrt{\langle y_\alpha^2/(y_{\max}-y_\alpha)^2\rangle}. \tag{5}$$

Finally, the transition between condensation (outlier) and demixing (bulk) regimes occurs when the two corresponding solutions for the spinodal temperature meet each other. Along the spinodal curve this condition defines a threshold density $\rho^*$ such that, for $\rho<\rho^*$, the spinodal is condensation-like and otherwise of demixing type.

Taken together, our results give a complete characterization of the spinodal line for any composition $p(y_\alpha)$ via Eq. (3), and of the nature of the spinodal instability via (4). In addition to the condensation-demixing transition [12], Eq. (5) reveals the novel possibility of *composition-driven demixing*, with instability directions $\boldsymbol{v}$ primarily determined by composition rather than the interaction pattern $\epsilon_{\alpha\gamma}$. We show below that this is not a simple entropic effect, but arises instead from an interplay between mixture composition and interaction complexity.

*Example 1: Uniform composition.*—The case where all mixture components have the same density has been studied in [12,23]. We revisit it briefly in order to illustrate our approach.

Since $y_\alpha\equiv 1$, Eq. (3) becomes $Tz(1-z\xi)/\rho=1$. Using that $z=\theta^{-1}$ in the condensation regime with $\theta=b-T/(1-\rho)$ gives a quadratic equation for the spinodal line $T(\rho)$. In the demixing regime, $T^*$ from Eq. (5) diverges so that thermodynamic stability is always governed by the interaction complexity $s\boldsymbol{\eta}$. One finds from the maximization condition [37] $z\xi=1-\xi/\tilde{s}$ which yields, using the spinodal equation, $T=2\tilde{s}\rho$.

To understand the nature of the instabilities we use Eq. (4). For uniform composition the first term is unity so one has condensation (C) as long as $\theta\equiv b-T/(1-\rho)>\tilde{s}$. This is the case at low densities, where $T$ and hence $T/(1-\rho)$ vanishes along the spinodal, provided that $b>\tilde{s}$. Therefore, at low densities $|\boldsymbol{v}^\mathsf{T}\hat{\boldsymbol{u}}|=O(1)$ with densities of all species changing by similar amounts at the spinodal instability. As the total density is increased, $\theta$ decreases and can approach $\tilde{s}$; $\boldsymbol{v}$ and $\hat{\boldsymbol{u}}$ then become orthogonal, resulting in random demixing (RD), with a delocalized instability vector $\boldsymbol{v}$ [35].

*Example 2: One dominant species.*—Next, we investigate the case of one single dominant species ($\alpha=1$) with relative concentration $y_1>1$, while all other species have $y_2\simeq 1$ (see [37] for $M$-dependent effects). This example will show how tuning the density of a few species can change the nature of the spinodal instability at high densities.

As discussed above, the single distinct entry in $\boldsymbol{D}$ results in a new type of demixing. Solving the spinodal equation (3) and computing the nature of the instability yields three different regimes depending on $y_1$ [37]. At low densities, the spinodal is dominated by the average interaction $-b$ and by entropic effects, yielding condensation behavior. Increasing $\rho$ results in a transition to demixing. We find explicitly for the instability direction in the demixing regime $|\boldsymbol{v}^\mathsf{T}\hat{\boldsymbol{u}}|=0$ and

$$|\boldsymbol{v}^\mathsf{T}\boldsymbol{e}_1|^2=\max\left\{\frac{y_1-2}{y_1-1},0\right\}, \tag{6}$$

where $\boldsymbol{e}_1=(1,0,0,\ldots,0)^\mathsf{T}$ indicates density changes only in the dominant species. The $O(1)$ overlap between $\boldsymbol{v}$ and $\boldsymbol{e}_1$ demonstrates that, whenever $y_1>2$, we have *composition-driven demixing* (CD) controlled by the dominant species. If, on the other hand, $y_1<2$ the instability is controlled by $s$ and the mixture will undergo random demixing. For $y_1>y_2$, the transition from C to CD happens at $\rho^*=1-y_1\tilde{s}/(b\sqrt{y_1-1}+\tilde{s})$ and the CD spinodal for $\rho>\rho^*$ follows $T=y_1\tilde{s}\rho/\sqrt{y_1-1}$.

In Fig. 2 we show the predictions for the spinodal curves for different $y_1$ and the corresponding instability direction; the comparison to results from numerical realizations of the Hessian matrix shows excellent agreement. For $y_1>2$ the instability vector is strongly concentrated on the dominant species at high densities, with $v_1/v_2=O(\sqrt{M})$. What is striking in this CD region is that the share of the dominant species in the instability direction is much larger than expected from entropic considerations, which would predict $v_1/v_2\sim y_1/y_2=O(1)$. This strong *composition imbalance amplification* is our key insight into instabilities in complex mixtures. It results from an interplay of entropic

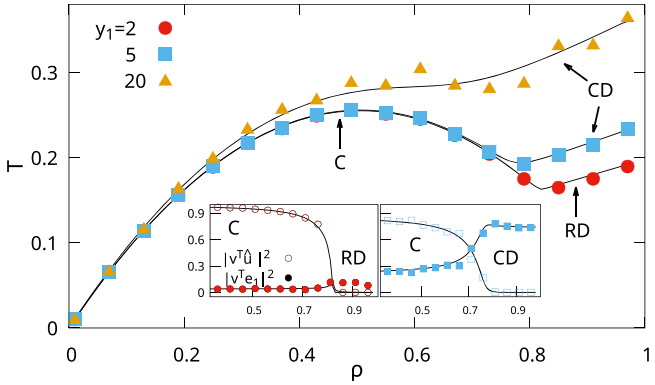


FIG. 2. Example 2: Spinodal lines for different $y_1 = \rho_1/\bar{\rho}$ at fixed $M = 100$, $s = 1$ and $b = 1$ (lines: theory, symbols: average over 50 numerical realizations of Hessian matrix). For $y_1 > 2$ the demixing is controlled by the dominant species. Insets: Projection of instability direction onto the constant vector $\hat{\boldsymbol{u}}$ and the dominant species direction $\boldsymbol{e}_1$, showing the transitions from C to RD and CD, respectively. We keep the $M$ dependence of $\theta$ in the theory to account for finite-size effects.

effects and interaction complexity ($\tilde{s} > 0$); indeed the CD regime would be absent in the limit $\tilde{s} \to 0$ (where $\rho^* \to 1$).

*Example 3: Beta distribution.*—We now turn to continuous distributions $p(y_\alpha)$ of relative densities and show how their shape affects instabilities. We focus on the beta distribution defined by

$$p(y) = Z_{r,t}^{-1}(y - y_{\min})^r(y_{\max} - y)^t, \qquad y \in [y_{\min}, y_{\max}] \quad (7)$$

with $Z_{r,t} = (y_{\max} - y_{\min})^{r+t+1}B(r+1, t+1)$ and $B(x, y)$ the beta function. The requirement $\langle y \rangle = 1$ reduces the number of free parameters to three out of $(y_{\min}, y_{\max}, r, t)$.

The spinodal equation (3) can be solved numerically in the condensation (C) region. More interesting here is the demixing regime. According to Eq. (5), for $T > T^*$ the demixing instability changes from being determined by the interaction complexity (RD) to being governed by the distribution of the $y_\alpha$ (CD). From Eq. (7),

$$T^* = \tilde{s}\rho y_{\max}\sqrt{(Z_{r,t-2}/Z_{r,t})\langle y^2\rangle_{r,t-2}}, \quad (8)$$

where $\langle\cdot\rangle_{l,m}$ denotes the average over the beta distribution (7) with exponents modified to $l$ and $m$ (but unchanged $y_{\min}$ and $y_{\max}$). For $T > T^*$ the spinodal equation (3) yields

$$T = \tilde{s}\rho y_{\max}\sqrt{(Z_{r,t-1}/Z_{r,t})\langle y\rangle_{r,t-1}}. \quad (9)$$

Comparing Eqs. (8) and (9), we see that whenever $Z_{r,t-1}\langle y\rangle_{r,t-1} > Z_{r,t-2}\langle y^2\rangle_{r,t-2}$ the demixing spinodal is dictated by the mixture composition. This condition for CD is independent of the total density and controlled only by the shape of $p(y)$. If e.g., we fix $y_{\min} = 0$ it reduces to $t > r + 3$, meaning that the upper edge of the distribution has a much longer tail than its lower edge. Thus, mirroring our results for example 2, composition-driven demixing occurs whenever a small fraction of species has significantly larger density than the average.

We can deduce from the results of Ref. [41] that the instability direction is delocalized across species in the RD regime ($T < T^*$). In the CD regime, it is concentrated on a few dominant species: these have entries of $O(1)$ in $\boldsymbol{v}$ and will, therefore, dictate the nature of the spinodal instability. Translating the results of [41] further to our context, the contribution of the highest-density species (denoted by $\boldsymbol{e}_1$) to the instability direction is $|\boldsymbol{v}^\mathsf{T}\boldsymbol{e}_1|^2 = 1 - (T^*/T)^2$, which is independent of $\rho$ along the CD spinodal. For the subsequent high-density species ($j > 1$) one has $|\boldsymbol{v}^\mathsf{T}\boldsymbol{e}_j|^2 \sim M^{-\gamma}$ with an exponent $\gamma > 0$ depending on the shape of $p(y)$.

The above results are the continuum analogs of the ones obtained in the single dominant species case: by changing the upper edge of the distribution $p(y)$ one can control the nature of instabilities, from delocalized to partially

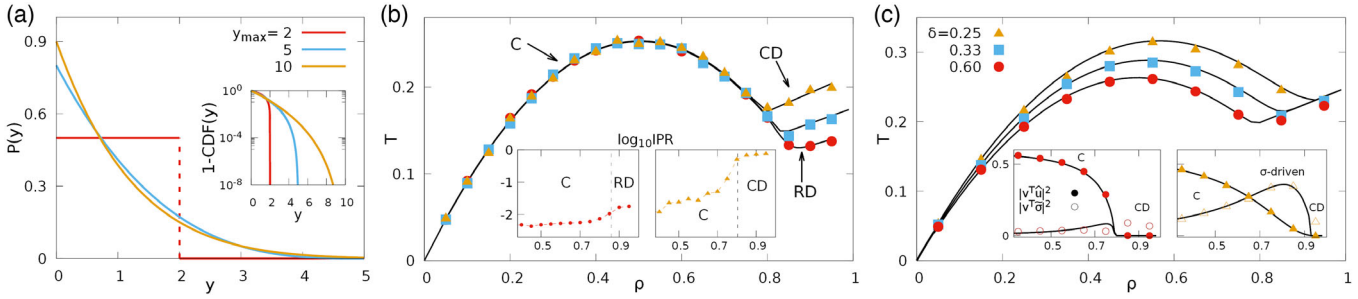


FIG. 3. (a) Beta distribution with $y_{\min} = 0$, $r = 0$ and $t = y_{\max} - 2$. The inset shows the complement of the cumulative distribution function, highlighting the different tail behaviors. (b) Spinodal line at fixed $M = 600$, $b = 1.0$, $s = 1.5$ for same distribution parameters (corresponding colors) as in (a). Inset: inverse participation ratio, showing the localization transition to CD on the right ($y_{\max} = 10$). (c) Spinodal lines for beta distribution with $y_{\max} = 5$ and systematic interactions, for different $\delta$. Inset: projection of instability direction onto the uniform vector $\hat{\boldsymbol{u}}$, and the remaining systematic interaction direction $\tilde{\boldsymbol{\sigma}} = \boldsymbol{\sigma} - \langle\sigma\rangle\boldsymbol{u}$; for small enough $\delta$ a new regime with instability direction dominated by systematic interactions ("$\sigma$-driven") appears.

concentrated onto a few dominant species. Figure 3 summarizes this example by showing the complete spinodal line in each regime. To demonstrate the localization of the instability direction onto the few dominant species, we also show the inverse participation ratio (IPR) along the spinodal. The IPR is defined as $\sum_\alpha v_\alpha^4$ and so of $O(M^{-1})$ for delocalized instabilities, while it reaches $O(1)$ when the instability is concentrated on a few species.

Here again one observes composition imbalance amplification in the CD regime: if purely entropic effects were at play, the components of the instability direction $\boldsymbol{v}$ should be distributed according to $p(y)$. This would yield a much lower IPR $[O(M^{-1})]$ than we find $[O(1)]$, cf. Fig. 3. The effect again requires $s > 0$, i.e., complexity in the underlying interactions.

Finally, we illustrate in Fig. 3(c) how the presence of systematic interactions creates further competition between different forms of demixing. We consider second virial coefficients of the form $\epsilon_{\alpha\gamma} = -b + s\eta_{\alpha\gamma} - \sigma_\alpha\sigma_\gamma$, with an additional systematic term parametrized by an interaction strength $\sigma_\alpha$ associated with each species, related to e.g., particle size or chemical composition. We write $\langle\sigma\rangle$ and $\mathrm{Var}_\sigma$ for the mean and variance of the $\sigma_\alpha$ and introduce the parameter $\delta = \tilde{s}/\sqrt{\mathrm{Var}_\sigma + \tilde{s}^2}$ measuring the relative strength of the random and systematic interactions. As density is increased, for sufficiently small $\delta$, the systematic interaction now dominates the instability, cf. Fig. 3(c). The inclusion of any finite number of similar systematic interactions into our framework is straightforward, thus allowing us [37] to extend existing models [14,42].

To conclude, we have provided a framework for understanding phase ordering instabilities in complex mixtures of arbitrary composition, which allows volume exclusion effects to be included as well as additional systematic interactions that would be expected in, e.g., polymeric mixtures [43,44] or colloids with charge or size polydispersity [30]. We have obtained an exact equation for the spinodal line in the limit of many components for typical mixtures with complex interactions [12]. In simple yet paradigmatic examples we showed that a small number of higher-density mixture components can strongly control the nature of instabilities through a surprising interplay between entropic effects and interaction complexity, resulting in a strong composition imbalance amplification. This new form of instability is our main physical insight and is a possible explanation for the strong composition dependence of phase behavior in biological experiments [18–20].

For systems above the spinodal but below the binodal line, phase separation proceeds via nucleation and growth. Even for uniform composition, determining the distinct composition of the new phase is highly nontrivial [7,8,30], even more so the appropriate surface tension [45]. Incorporating additionally the effects of non-uniform system composition is an important task for the future using, e.g., expansions around the critical point [8,42]. Our approach can also be extended to understand the composition dependence of the number of negative eigenvalues inside the spinodal region, which has been conjectured [11] to control the number of phases formed. Since in many biological mixtures different components are present in different amounts, we expect instabilities to phase separation in such systems to be generically dictated by the components with the highest concentration. Our results thus point to a new route for biological systems to control patterns of phase separation by fine-tuning mixture composition imbalances.

This work was supported by the German Research Foundation (DFG) under Grants No. SO 1790/1-1 and No. KR 3844/5-1.

*Corresponding author.
filipe.cunhathewes@uni-goettingen.de

[1] S. Alberti, Curr. Biol. **27**, R1097 (2017).
[2] D. L. J. Lafontaine, J. A. Riback, R. Bascetin, and C. P. Brangwynne, Nat. Rev. Mol. Cell Biol. **22**, 165 (2020).
[3] R. P. Sear, Soft Matter **3**, 680 (2007).
[4] J. Berry, C. P. Brangwynne, and M. Haataja, Rep. Prog. Phys. **81**, 046601 (2018).
[5] J.-M. Choi, A. S. Holehouse, and R. V. Pappu, Annu. Rev. Biophys. **49**, 107 (2020).
[6] C. D. Keating, Acc. Chem. Res. **45**, 2114 (2012).
[7] W. M. Jacobs and D. Frenkel, J. Chem. Phys. **139**, 024108 (2013).
[8] W. M. Jacobs and D. Frenkel, Biophys. J. **112**, 683 (2017).
[9] W. M. Jacobs, Phys. Rev. Lett. **126**, 258101 (2021).
[10] D. Zwicker and L. Laan, Proc. Natl. Acad. Sci. U.S.A. **119**, e2201250119 (2022).
[11] K. Shrinivas and M. P. Brenner, Proc. Natl. Acad. Sci. U.S.A. **118**, e2108551118 (2021).
[12] R. P. Sear and J. A. Cuesta, Phys. Rev. Lett. **91**, 245701 (2003).
[13] E. P. Wigner, Math. Proc. Cambridge Philos. Soc. **47**, 790 (1951).
[14] G. Carugno, I. Neri, and P. Vivo, Phys. Biol. **19**, 056001 (2022).
[15] R. P. Sear, J. Phys. Condens. Matter **17**, S3587 (2005).
[16] A. G. Gasic, A. Sarkar, and M. S. Cheung, Phys. Rev. Res. **3**, 033220 (2021).
[17] *Escherichia coli and Salmonella typhimurium: Cellular and Molecular Biology*, edited by F. C. Neidhardt, S. L. Ingraham, K. B. Low, B. Magasanik, M. Schaecter, and H. E. Umbarger (American Society for Microbiology, Washington, DC, 1987), pp. 3–6.
[18] S. C. Weber and C. P. Brangwynne, Curr. Biol. **25**, 641 (2015).
[19] N. W. Goehring and A. A. Hyman, Curr. Biol. **22**, R330 (2012).
[20] J. A. Riback, L. Zhu, M. C. Ferrolino, M. Tolbert, D. M. Mitrea, D. W. Sanders, M.-T. Wei, R. W. Kriwacki, and C. P. Brangwynne, Nature (London) **581**, 209 (2020).
[21] H. Zhang, S. Elbaum-Garfinkle, E. M. Langdon, N. Taylor, P. Occhipinti, A. A. Bridges, C. P. Brangwynne, and A. S. Gladfelter, Mol. Cell **60**, 220 (2015).

[22] A. W. Fritsch, A. F. Diaz-Delgadillo, O. Adame-Arana, C. Hoege, M. Mittasch, M. Kreysing, M. Leaver, A. A. Hyman, F. Jülicher, and C. A. Weber, Proc. Natl. Acad. Sci. U.S.A. **118**, e2102772118 (2021).
[23] J. Moran and J.-P. Bouchaud, Phys. Rev. E **100**, 032307 (2019).
[24] E. Bouchbinder, E. Lerner, C. Rainone, P. Urbani, and F. Zamponi, Phys. Rev. B **103**, 174202 (2021).
[25] I. Neri and F. L. Metz, Phys. Rev. Res. **2**, 033313 (2020).
[26] S. Allesina and S. Tang, Popul. Ecol. **57**, 63 (2015).
[27] S. Allesina and S. Tang, Nature (London) **483**, 205 (2012).
[28] J. W. Baron and T. Galla, Nat. Commun. **11**, 6032 (2020).
[29] C. A. Weber, D. Zwicker, F. Jülicher, and C. F. Lee, Rep. Prog. Phys. **82**, 064601 (2019).
[30] P. Sollich, J. Phys. Condens. Matter **14**, R79 (2001).
[31] G. Akemann, J. Baik, and P. Di Francesco, *The Oxford Handbook of Random Matrix Theory* (Oxford University Press, New York, 2011).
[32] T. Tao and V. Vu, Acta Math. **206**, 127 (2011).
[33] Only if the entries of $\boldsymbol{D}$ are relatively close to each other. Otherwise, the spectrum may split into multiple bulk pieces.
[34] S.-G. Hwang, Am. Math. Mon. **111**, 157 (2004).
[35] F. Benaych-Georges and R. R. Nadakuditi, Adv. Math. **227**, 494 (2011).
[36] D. V. Voiculescu, K. J. Dykema, and A. Nica, *Free Random Variables* (American Mathematical Society, Providence, 1992), Vol. 1.
[37] See Supplemental Material at http://link.aps.org/supplemental/10.1103/PhysRevLett.131.058401 which contains Refs. [38–41] for details of derivations and discussion of the effects of finite number of mixture components.
[38] Z. Burda, J. Phys. Conf. Ser. **473**, 012002 (2013).
[39] Z. Bai, B. Miao, and J. Tsay, J. Theor. Probab. **12**, 301 (1999).
[40] L. A. Pastur, Theor. Math. Phys. **10**, 67 (1972).
[41] J. O. Lee and K. Schnelli, Probab. Theory Relat. Fields **164**, 165 (2016).
[42] I. R. Graf and B. B. Machta, Phys. Rev. Res. **4**, 033144 (2022).
[43] I. Pagonabarraga and M. E. Cates, Macromolecules **36**, 934 (2003).
[44] C. Grodon and R. Roth, J. Chem. Phys. **126**, 054901 (2007).
[45] S. Auer and D. Frenkel, Nature (London) **413**, 711 (2001).